European Office of Aerospace Research and Development

Contract NO FA8655-04-1-3042

Terahertz radiation emitters from narrow-gap semiconductors

Final report

Contractor:
Semiconductor Physics Institute
A. Gostauto 11, Vilnius, Lithuania

Principal investigator:
Prof. Arunas Krotkus
Head of the Optoelectronics Laboratory

Vilnius   2005

REPORT DOCUMENTATION PAGE

Form Approved OMB No. 0704-0188

1. REPORT DATE *(DD-MM-YYYY)*	2. REPORT TYPE		3. DATES COVERED *(From – To)*
01-08-2005	Final Report		1 June 2004 - 25-Aug-05

4. TITLE AND SUBTITLE

Terahertz Radiation Emitters From Narrow-Gap Semiconductors

5a. CONTRACT NUMBER
FA8655-04-1-3042

5b. GRANT NUMBER

5c. PROGRAM ELEMENT NUMBER

6. AUTHOR(S)

Professor Arunas Krotkus

5d. PROJECT NUMBER

5d. TASK NUMBER

5e. WORK UNIT NUMBER

7. PERFORMING ORGANIZATION NAME(S) AND ADDRESS(ES)
Semiconductor Physics Institute
A.Gostauto 11
Vilnius 2600
Lithuania

8. PERFORMING ORGANIZATION REPORT NUMBER

N/A

9. SPONSORING/MONITORING AGENCY NAME(S) AND ADDRESS(ES)

EOARD
PSC 802 BOX 14
FPO 09499-0014

10. SPONSOR/MONITOR'S ACRONYM(S)

11. SPONSOR/MONITOR'S REPORT NUMBER(S)
Grant 04-3042

12. DISTRIBUTION/AVAILABILITY STATEMENT

Approved for public release; distribution is unlimited.

13. SUPPLEMENTARY NOTES

14. ABSTRACT

This report results from a contract tasking Semiconductor Physics Institute as follows: The grantee will investigate optimizing material parameters of low-temperature grown GaAs for efficient THz emitters and detectors.

15. SUBJECT TERMS
EOARD, terahertz electronics

16. SECURITY CLASSIFICATION OF:			17. LIMITATION OF ABSTRACT	18, NUMBER OF PAGES	19a. NAME OF RESPONSIBLE PERSON
a. REPORT	**b. ABSTRACT**	**c. THIS PAGE**	UL		DONALD J SMITH
UNCLAS	UNCLAS	UNCLAS		38	**19b. TELEPHONE NUMBER** *(Include area code)* +44 (0)20 7514 4953

Standard Form 298 (Rev. 8/98)
Prescribed by ANSI Std. Z39-18

Table of contents

Executive summary

When illuminated with femtosecond laser pulses, the majority of the semiconductor surfaces radiate electromagnetic transients with characteristic frequencies far into the terahertz (THz) frequency range. Most efficient THz emitters are semiconductors with narrow energy band gaps, in which the electrons are excited by the absorbed light at large excess energies.

In the present work, THz emission from several narrow gap semiconductors: InAs, InSb, $Cd_xHg_{1-x}Te$, and Ge are studied both experimentally and theoretically. Relative roles of different physical THz generation mechanisms are compared by employing measurements performed on differently doped samples and under various experimental conditions. It has been demonstrated that in $Cd_xHg_{1-x}Te$ and Ge the prevailing mechanism of THz emission is the photo-Dember effect arising due to differing photoexcited electron and hole group velocities, whereas in InAs and InSb the shift current effect is dominating.

Spectral dependencies of the optical to THz conversion efficiency are investigated in InAs and InSb by using femtosecond laser pulses tunable over a wide wavelength range from 600 nm to 2100 nm; it has been found that the conversion efficiency in the case of laser illuminated InAs surfaces peaks at 800 nm and 1300 nm, whereas InSb is the best THz emitter for the laser wavelengths ranging from 1400 nm to 2000 nm.

The effect of THz radiation from the semiconductor surfaces was used also for determining important parameters of the investigated materials: intervalley energy separation in InSb and InAs and intervalley phonon deformation potential in Ge.

1. Introduction. THz generation from the semiconductor surfaces illuminated by femtosecond laser pulses.

There is presently an enhanced interest in generation of intense, coherent terahertz (THz) beams spanning the so-called "Terahertz gap" range of the electromagnetic spectrum from ~100 GHz to ~10 THz. As yet, there are no compact semiconductor sources of THz radiation within this frequency range. The largest breakthrough in generation of coherent and broadband pulses of electromagnetic radiation of THz frequency range is achieved by using ultrashort laser pulses illuminating semiconductor surfaces [1-4]. There are quite a number of different physical mechanisms that are employed for this generation; they could be divided into three groups. Coherent THz pulses are generated by the semiconductor illuminated by femtosecond laser pulses due to:

  i) nonlinear optical interaction between the light pulses and the material,

  ii) photocurrent surge perpendicular to the illuminated surface, and

  iii) lateral photocurrent effect using wideband antennae integrated with photoconductors made from the semiconductor with ultrashort carrier lifetimes.

The later effect is negligible in narrow-gap semiconductors because of their intrinsically low resistivity; therefore, in the following, we will shortly describe only two former physical mechanisms and compare the characteristics of THz radiation beams obtained by using different ultrafast optoelectronic approaches.

1.1 Optical rectification.

The optical rectification approach uses electro-optic crystals as a rectification medium and, depending on the optical fluence, the rectification is a second order (difference frequency generation) or a higher order nonlinear optical process. Conventional optical rectification usually refers to the generation of dc electric polarization by an intense optical beam in a nonlinear medium. In the THz optical rectification process, an ultrafast laser pulse creates in a nonlinear optical medium a beating polarization due to the spectral broadening of the laser pulse due to the uncertainty principle. Pulsed electromagnetic waves are then radiated by the time varying polarization of a transient electrical dipole.

In the case of zinc-blende single crystals like GaAs or InAs, no optically induced THz radiation from unbiased semiconductor is observed when the illumination is at a normal incidence at (100) planes. However, for (110) GaAs, a signal with a three-fold rotational symmetry around the surface normal was observed and interpreted as evidence of the optical rectification process [5].

In fact, when optical beams are resonant with valence-to-conduction band transitions, i.e., with frequencies higher than that associated with the band gap of the material (as it is in the case of GaAs excited by Ti:sapphire laser pulses, which is the most popular experimental situation), the underlying physics of the dc response is more complicated.

It has been shown by Sipe and Shkrebtii [6] that if a pulse with centre frequency ω_0 and temporal electric field envelope $E(t) = \int d\omega\, \tilde{E}(\omega)e^{-i(\omega-\omega_0)t}$ interacts with a semiconductor, the components $\tilde{E}$ and $\tilde{E}(\omega-\Omega)$ induce a nonlinear polarization $\tilde{P}(\Omega)$ via a second order optical nonlinear susceptibility χ_2, which contains three contributions:

$$\chi_2(-\Omega;\omega,-\omega+\Omega) = \chi_2^{/}(-\Omega;\omega,-\omega+\Omega) + \frac{\sigma_2(-\Omega;\omega,-\omega+\Omega)}{-i\Omega} + \frac{\eta_2(-\Omega;\omega,-\omega+\Omega)}{(-i\Omega)^2}. \qquad (1)$$

The first term represents the nonresonant (rectification) component and reflects displacement of virtually excited carriers; it is nonzero for all ω. The other two terms are associated with the production of carriers in the resonantly excited bands and lead to electrical current. The second term (containing σ_2, which is purely real) arises from the spatial shift of the center of charge during excitation and leads to a "shift" current. Finally, the third term containing η_2 reflects quantum interference between different pathways involving different polarization components of the same beam and linking the same initial and final states in the valence and conduction bands. For materials with an appropriate symmetry it can lead to injection of a polar distribution of carriers. This injection current vanishes in a zinc-blende structure like GaAs, although it survives in lower symmetry materials such as those of the wurtzite structure.

Contributions of the second-order rectification and shift currents in GaAs at 295 K were compared experimentally in [7] by using 150 fs pulses at 1.55 and 0.775 μm, respectively. It has been found that for the same, low pump intensity of 100 MW/cm^2, the shift current is 570 times larger than the rectification current density. At high intensities, the shift current is strongly affected by the carrier screening and the dephasing phenomena.

When a built-in electrical field E_0 is present at the surface of the semiconductor, similar effects can occur also due to the third order optical nonlinearity, which, in the presence of E_0 leads to effective second order nonlinearity

$$\chi_3(-\Omega;\omega,-\omega+\Omega, E_0) = \chi_2(-\Omega;\omega,-\omega+\Omega)E_0 \qquad . \qquad (2)$$

In zinc-blende crystals both pure and electric-field induced second order nonlinearities have analogous dependences on the crystallographic direction; therefore their separation from a single azimuthal angle dependence measurement is impossible.

1.2 Surface field.

In the surface field photocurrent model, THz radiation is generated when the electron-hole pairs, created by the visible pump beam, are accelerated by the surface electric field, E_{surf}, which is shown schematically in Figure 1. The resulting transient photocurrent j leads to the radiation at THz frequencies [2,8]. This effect has been shown to be effective at ultrafast laser pulse illuminated surfaces of GaAs [2] and InP [9]; especially strong THz radiation caused by the surface field photocurrent was observed in the case of InN [10].

Fig. 1 Schematic representation of the THz generation by the surface photocurrent effect.

Many studies have shown that, in a surface electric field, the total THz signal generated can be significantly enhanced by application of a magnetic field. It has been demonstrated [11] that the critical effect of the magnetic field consists of a change in the direction of the carrier movement. Due to the large difference in refractive indexes at the air-semiconductor interface, this change of direction determines a significant enhancement in the transmission of the radiated THz through this interface and in more efficient coupling of the THz radiation out of the sample. Similar magnetic field influence cannot be imagined when the THz radiation is caused by some of the nonlinear optical effects, therefore the magnetic field measurement presents a test for distinguishing photocurrent surge and optical rectification mechanisms.

1.3 Photo-Dember effect.

Surface band bending and surface electric field in narrow-gap semiconductors should, generally, be rather weak, nevertheless these semiconductors, when excited by ultrafast laser pulses, also emit THz radiation quite efficiently. One of such semiconductors - indium arsenide, is known as the best THz emitter of all semiconductors [12]. THz emission was also observed from the surfaces of narrow-gap InSb [13], InGaAs [14], and Te [15].

Those observations were explained in [15] by the occurrence of the so-called photo-Dember effect. In a typical semiconductor, electrons have a larger diffusion coefficient than holes. After photoexcitation, the electron population diffuses more rapidly that the hole population but in the absence of a surface boundary, there is no net dipole field, since the centre of charge does not change. In the vicinity of the surface, however, reflection or capture causes the net electron and hole charge centres to move away from the surface. The greater diffusivity of the electrons produces a perpendicular dipole which leads to THz emission.

THz emission due to the photo-Dember effect is affected by the external magnetic field in a similar way as in the case of the surface-field photocurrent effect. Due to the large electron mobility of narrow-gap semiconductors, in which the photo-Dember effect is dominating, the radiated from these materials THz power can be enhanced by the magnetic field by several orders of magnitude – much more than, e.g., in GaAs, when the surface-field photocurrent mechanism is prevailing. There are also several other differences between the characteristic features of those two physical mechanisms of THz emission.

If the photo-Dember effect is dominant, the polarity of the radiated THz waveform will remain the same for n-type and p-type samples because the direction of carrier diffusion will not change with the type of doping, while in the case of the surface-field effect the polarity will flip depending on the type of doping because the depletion field direction flips according to doping type. Lastly, important differences should be observed also by comparing the excitation-wavelength dependences of these two THz emission mechanisms. In general, THz transients caused by the surface-field photocurrent should be less sensitive to the value of this parameter, whereas the Dember voltage V_D is proportional to the temperature of the hot, photoexcited electrons T as [16]

$$V_D = \frac{k_B T}{e} \cdot \frac{b-1}{b+1} \cdot \ln(1 + \frac{(b+1)\Delta n}{n_0 b + p_0}) \tag{1}$$

where b is the electron to hole mobility ratio, Δn is the photoexcitated carrier density, n_0 is the equilibrium electron and p_0 is the equilibrium hole densities. Shortening of the laser wavelength will, therefore, lead to the increase of the excess energy and the temperature of the photoexcited electrons and, thus, to enhanced V_D.

On the other hand, when the excess energy will be greater than the intervalley energy separation in the conduction band, the excited electrons will be efficiently scattered to the subsidiary, high electron effective mass valleys, their transport parameters will be severely reduced, and the magnitude of the THz transients will decrease. Such intervalley transfer of electrons is supposed to be responsible for unexpectedly weak THz emission from high-mobility InSb crystals [17].

1.4 Plasma oscillations.

Another concept of THz radiation from semiconductor surfaces is coherent plasma oscillations of charge carriers. The charge carriers are bound by their Coulomb potential and the plasma frequency depends on the carrier density. Since the oscillating current density of the plasmons leads to the emission of an electric field $E_{rad} \sim (\partial/\partial t)j(t)$, plasma oscillations should emit submilimeter or THz wave radiation. Evidence of coherent plasmons was obtained by time-resolved pump-and-probe experiments in p-i-n diodes [18], accumulation layer of a GaAs heterostructure [19], and in bulk GaAs layers [20].

After photogeneration, nonequilibrium electrons and holes start a drift motion in the surface field region or diffuse at different speeds if such a field is absent. As a result of the Coulomb attraction between the oppositely charged carriers a polarization is built up that counteracts the initial carrier separation. The polarization leads to a restoring force of the carrier motion and thus to an oscillating motion of the charge carriers at the frequency $\omega = \sqrt{\omega_p - \gamma^2/4}$, where γ is the damping rate of the oscillation. For small wave vectors k the plasma frequency ω_p of the volume plasmon is given by

$$\omega_p = \sqrt{\frac{e^2 n}{\varepsilon m^*}} \qquad (3)$$

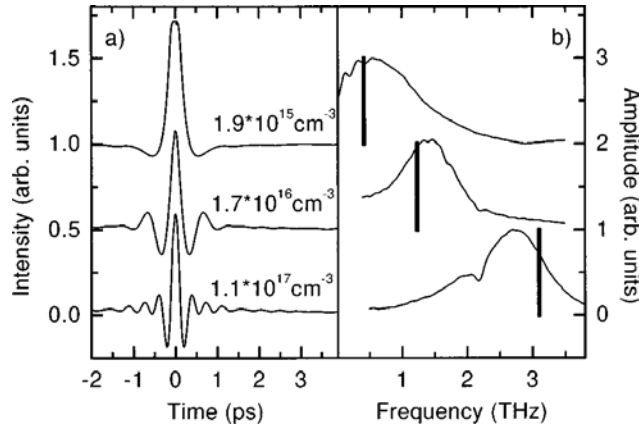where n is the density of the oscillating carriers and m is their effective mass.

Fig. 2 (a) Correlation data recorded on GaAs structures n-doped at $1.9 \cdot 10^{15}$, $1.7 \cdot 10^{16}$, and $1.1 \cdot 10^{17}$ cm^{-3}. (b) Fourier spectra. The bars indicate the calculated plasma frequencies.

Fig. 2 shows the results of the correlation type measurement of THz transients and their fast-Fourier-transform spectra obtained on three n-GaAs samples with differing equilibrium carrier concentrations. The vertical bars on the spectra indicate the plasma frequencies calculated for corresponding carrier concentrations. Observed shift of the maximum of the THz radiation spectrum with the increase of the carrier concentration is a typical signature of the plasma-oscillation effect.

It has been proposed in [20] to improve the performance of n-GaAs plasmon emitters by placing an additional layer grown by molecular-beam-epitaxy at low temperature (LTG GaAs) on

top of n-doped layer. It is expected that a thin LTG GaAs layer should ensure a firm pinning of the Fermi level in the middle of the GaAs bandgap, thus increasing the emitted power of the THz radiation and providing better long term stability when compared to an emitter without LTG GaAs surface layer. The best results in that respect were obtained in [21] where as-grown, Be-doped LTG GaAs layers were used for the surface modification. The THz power of the surface-modified emitters was up to 4 times larger than of the reference devices.

1.5 Coherent phonon emission.

In [22], Kuznetsov and Stanton have theoretically investigated coherent optical phonons excited in GaAs and predicted that longitudinal optical (LO) phonon oscillations of IR-active mode would emit terahertz radiation. Such modes excited in a finite-size volume would produce oscillating macroscopic dielectric polarization. This will lead to the appearance of a Hertzian dipole emitting electromagnetic waves with the LO phonon frequency [22]. Soon after this prediction was made, Dekorsy et.al [15] observed a pronounced THz radiation from coherent LO phonons of the IR-active A2 mode excited in tellurium single crystal. They also observed an absence of radiation component at the frequency of the transverse optical (TO) phonons. The frequency of A2 LO-mode in Te is 2.82 THz and the frequency of the TO mode is 2.6 THz.

Later on, THz emission due to the coherent phonon oscillations was observed in two other Te-containing materials: PbTe and CdTe [23]. Optical phonon modes in these telluride crystals are at relatively low frequencies (3.42 THz and 5.08 THz for LO modes in PbTe and CdTe, respectively) allowing to measure the THz radiation from the coherent phonons with a high-speed photoconductive detector. Figure 3 shows Fourier-transformed amplitude spectra of the THz transient measured by ultrafast photoexcitation of three different materials [23]. The TO and LO frequencies of each material are indicated by vertical arrows. In Te and CdTe crystals lower frequency part of the spectra are dominated by photo-Dember and surface field type emission, respectively, whereas for PbTe the coherent
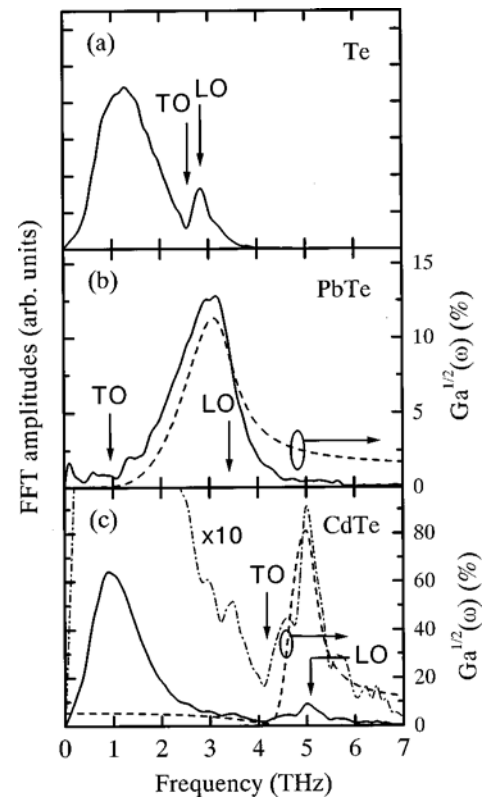
Fig. 3. Fourier-transformed amplitude spectra of the THz transients in Te, PbTe, and CdTe [23].

phonon effect is the main cause of THz radiation. The surface field in this material is small because of the narrow bandgap; the efficiency of the photo-Dember effect, on the other hand, is reduced because electron and hole mobilities and diffusion coefficients in PbTe are of the same order of magnitude.

1.6 Objectives of the work.

Semiconductor surfaces illuminated by femtosecond laser pulses can emit THz radiation due to a number of different physical effects. Some of the semiconductors especially narrow gap materials like InAs can generate quite large THz power that could be used in various applications. However, even in the case of InAs – the material in which THz radiation was studied more often than in other narrow gap semiconductors – the physical mechanism leading to this effect is far from being fully understood and a further investigation is necessary.

Therefore, *the first objective of the work is the investigation of the physical mechanisms leading to THz radiation from narrow gap semiconductor surfaces illuminated by femtosecond laser pulses and the optimization of the performance of THz emitters manufactured from these semiconductors*.

The majority of the investigations of THz emission from laser illuminated semiconductor surfaces were, as yet, performed by employing near-infrared femtosecond pulses generated by the mode-locked Ti:sapphire lasers. These lasers are widely available commercially, reliable, and stable, however, there are not optimal for the applications in THz radiation systems. Ti:sapphire lasers are quite bulky, inefficient, and require two stage optical pumping. On the other hand, recently new more compact and efficient femtosecond laser systems like fiber lasers or Cr:forsterite lasers appeared, which are prospective for applications in THz radiation systems. However, the light wavelengths generated by these lasers are longer (1-1.5 μm) than that of Ti:sapphire laser, therefore, new semiconductor materials for THz emitters and detectors should be sought.

The second objective of this work was, thus, spectral measurements of THz emission from narrow gap semiconductors and the search for new materials that can emit THz radiation when excited by long wavelength laser pulses.

Finally, the investigation of THz emission from laser excited semiconductor surfaces can provide a wealth of new information on the parameters of the material. *The use of THz emission for the study of narrow gap semiconductors will be an additional objective of this work*. In

particular, this emission was employed for the determination of the parameters of the subsidiary conduction band valleys: their energy position and the electron intervalley scattering rates.

2. Experimental techniques

2.1 THz transient measurements

Below, we will present the results of THz radiation measurements from laser excited surfaces of $Cd_xHg_{1-x}Te$, InAs and Ge samples. THz pulse magnitude has been investigated as a function of the alloy composition of $Cd_xHg_{1-x}Te$ and the doping level of InAs and Ge. THz emission from $Cd_xHg_{1-x}Te$ alloys was observed for the first time; only a short mention on its observation was available also in the case of Ge crystals [2]. More extensive are the data on THz radiation from femtosecond laser excited InAs surfaces, however it was not until our work that the dependence of this effect on the crystal doping level was studied in detail.

Fig. 4. Set-up for measuring THz emission from the semiconductor surfaces.

Samples of $Cd_xHg_{1-x}Te$ with x= 0; 0,2; and 0,3 have been investigated. The sample of HgTe was single crystalline, whereas the samples of remaining two alloy compositions were epitaxial layers grown on CdTe substrates. THz radiation was observed from photoexcited (100) surfaces.

Single crystalline samples of n- and p-type InAs corresponded to the doping ranges from 10^{16} cm^{-3} to 10^{19} cm $^{-3}$. In this case THz radiation was generated by mechanically polished (111) surfaces of the material.

Single crystalline samples of n- and p-type germanium corresponded to the doping ranges from 3×10^{14} cm^{-3} to 10^{19} cm $^{-3}$. In this
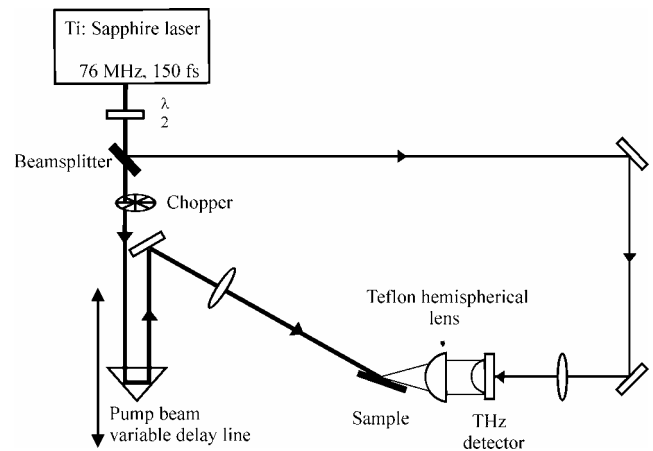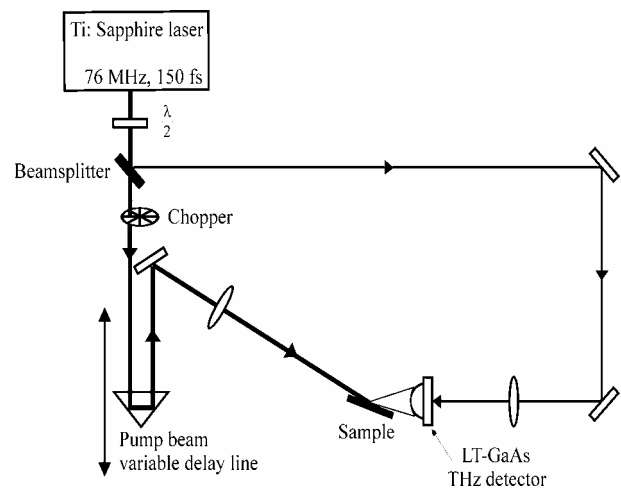
Fig. 5. Simplified set-up for measuring THz emission from the semiconductor surfaces.

case THz radiation was generated by mechanically polished (111) surfaces of the material.

Ti:sapphire laser pulses (pulse duration of 150 fs, pulse repetition rate of 76 MHz, central wavelength of 800 nm, and average power of 500 mW) were used for the sample's excitation. Radiated THz transients were registered by ultrafast photoconductor manufactured from low-temperature-grown GaAs epitaxial layer. The laser beam was split in two parts; one of the parts was used for the photoexcitation of the semiconductor surface, whereas the second part was opening the ultrafast photoconductor. Generated THz transient was temporally sampled by changing the delay between the pulses in two laser beam parts. This transient was directed towards ultrafast photoconductor by using two off-axis parabolic mirrors or a Teflon lens (Fig. 4). In some of the experiments, the samples were placed in the vicinity of the detector without any additional optical components (Fig. 5).

When measuring spectral dependencies of THz emission efficiency, samples made from InSb (nominally undoped, $n = 2 \times 10^{16}$ cm^{-3}, $\mu = 6 \times 10^4$ cm^2/V sec) and n-InAs ($n = 2.2 \times 10^{16}$ cm^{-3}, $\mu = 4.3 \times 10^4$ cm^2/V sec) single crystals were investigated. THz emission was observed from mechanically polished (111) surfaces. 150 fs duration, 1 kHz repetition rate tunable central wavelength pulses were used for the sample excitation. The pump laser power was $\approx$10 mW (10 μJ/pulse), and the pump beam diameter at the sample surface was 8.5 mm. The pump beam was incident at 45° to the sample surface. Nearly collinear THz beam was emitted along the direction of the reflected pump beam. THz radiation was focused by means of Teflon lens and registered by a photoconductive detector. The detector was oriented to prevailingly register TM polarization of the radiated emission and was manufactured from the layer of GaAs that was grown by molecular-beam-epitaxy at low (~250 ^{o}C) substrate temperature and has an electron trapping time less than 500 fs.

Experiments were performed by using optical pulses from an optical parametric amplifier and amplified Ti:sapphire laser system. The duration of the laser pulses was 100 fs, the central wavelength was 805 nm, the single pulse energy was 1 mJ, and the pulse repetition rate was 1 kHz. The laser beam was split into two parts, the smaller of which was sent through the optical delay line to gate THz detector and the larger was used to pump parametric amplifier. Optical parametric generation was based on type II phase-matched BBO crystal. Collinearly propagating tunable wavelength *signal* and *idler* beams were generated inside that crystal. The tuning ranges of *signal* and *idler* were 1200 nm – 1610 nm and 1610nm -2440 nm respectively. To obtain a radiation with the wavelengths around 800 nm, second harmonic generation using the *signal* or the *idler* beams was used. Tuning range of the second harmonic waves was 600 nm – 930 nm. Required

wavelengths were selected by a set of dichroic mirrors; the sample's excitation power P(λ) was kept nearly constant by means of neutral filter attenuator.

2.2 Optical pump – THz probe technique

The setup for the optical pump-terahertz probe experiment is shown schematically in Fig.6. A Ti:sapphire laser (Mira 900, Coherent) produced a 76-MHz repetition rate pulse train of 8 nJ, 800 nm pulses of 150 fs duration. Each pulse is split into three parts, each of which is responsible for THz emitter, detector, or optical photoexcitation arms of the spectrometer.

Photoconductive antennas are used for the generation and detection of THz pulses. The THz pulses are generated at the emitter when the pulse of 800 nm light excites carriers into the conduction band of the LTG GaAs layer. The width of the radiated pulse depends mainly on the duration of the optical pulse. The detector consists of a transmission line bridged by an antenna with a gap in the centre. Its operation is similar to the emitter, except that rather than applying a dc bias voltage; the transient THz field itself provides the bias voltage. If the gap is gated by the visible pulse when there is a large THz field, carriers will move from one side of antenna to the other. The material
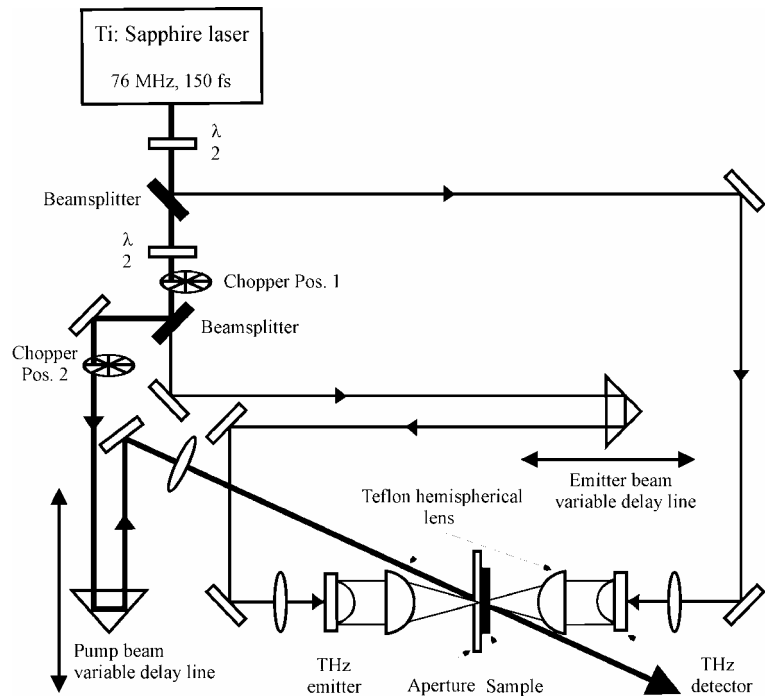

Fig. 6. The setup for the optical pump-terahertz probe experiment

used for the detector (LTG GaAs) has a very short carrier lifetime. Charge flows through the registration circuit in proportion to the amplitude of the THz field at the moment when the visible pulse gated the detector. The full waveform is mapped out by stepping the variable delay line incrementally. The sign of the field is determined in addition to its magnitude. The signal is collected with a lock-in amplifier (Stanford Research systems SR530) phase-locked to an optical chopper which modulates either the THz generation arm or the pump beam.

The 200 μm or 300 μm pinholes were used to overlap the THz and visible beams at the sample. The spot size of the pump beam was larger than diameter of the pinhole, so that the THz probe beam was sampling a uniformly photoexcited region. To maximize the transmitted through the pinhole power, the THz beam was focused before and collimated after the pinhole by two hemispherical Teflon lenses. Focused to 50-μm-diameter optical beams were used for THz generation and detection. The average power used for THz detection was 45 mW. The rest of the laser beam power was distributed between THz generation and optical excitation arms. The proportion of this distribution was changed by means of λ/2 plate and a polarizing beamsplitter.

The optical pump-terahertz probe experiment includes three stages. The first stage of the experiment is carried out by chopping THz generation arm and scanning the emitter beam delay line to map out the THz pulse. The optical pump beam is blocked. The second stage of the experiment are performed by chopping the optical pump beam, fixing emitter beam delay line at the position corresponding to the highest point on the THz waveform, and scanning the optical pump delay line to vary the arrival time of the pump pulse relative to the THz probe pulse. The THz transmission kinetics and THz generation from the surface of the sample can be seen from the measured trace. The third stage of the experiment is performed by repeating the earlier procedure with the blocked THz emitter beam. The THz generation from the surface of the sample can be seen from the measured trace. The final trace we can get by extracting the third trace from the second. This yields information about decay of photoconductivity in semiconductors.

3. Results

3.1 Physical mechanism of THz emission from InAs

3.1.1. Experiments on variously doped InAs crystals.

Most efficiently THz radiation is generated from the surface of InAs crystals, especially when a strong magnetic field is applied in parallel to those surfaces [12]. This enhanced magnetic field influence (magnetic fields of ~1 T can lead to an increase of the emitted THz power by a factor of 100) had focused the attention of researchers on the photo-Dember effect, although some authors have also pointed out the role of other phenomena like bulk optical rectification [17], magneto-plasma waves [24], or coupled plasmon-phonon modes [25] in THz radiation from InAs surface. Possible influences of the surface electric field were usually written off due to a narrow band gap in InAs and potentially small band bending at the surface of this material. This is not always justifiable, because it is known that surface potential in InAs is fixed at fairly high (0.18-0.2 eV [26]) values and in an appropriately doped crystal surface depletion layer can be sufficiently wide

and strong. However, no systematic investigation of THz radiation in differently doped InAs was performed until yet; in the majority of references only nominally undoped or lightly doped (electron or hole density of the order of 10^{16} cm^{-3}) InAs crystals were used. More systematic study of the doping effect was performed in [17], although only n-doped crystals were also considered in that work.

Fig.7. Dependence of the emitted THz field magnitude on the InAs crystal doping level.

In the present work we measured THz radiation emitted from laser illuminated surfaces of a large number of variously doped InAs crystals. A strikingly strong doping dependence (THz power varying over more than two orders of magnitude) and enhanced sensitivity of some samples to the crystalline orientation let us to conclude that the effect of the instantaneous polarization at laser irradiated InAs surfaces is comparable and, in some cases, even prevailing cause of strong THz radiation from this material.

Fig. 7 shows the dependence of the emitted THz field magnitude on the crystal doping level. It can be seen from that Figure that there is a strong enhancement of the radiated field magnitude corresponding to p-type doping levels of 10^{16} to 10^{17} cm^{-3}. The shape of THz transients recorded in

the range with the largest magnitudes is very sensitive to the azimuthal angle of the sample orientation around the axis normal to the surface. This is demonstrated by two azimuthal dependences shown on Fig. 8. for the sample with p-doping level from the range with the maximal THz amplitudes, azimuthal dependence is very pronounced – the ratio of the signals at the angles corresponding to their maxima and minima reaches 20, whereas for n-InAs this ratio is close to the value of 2, which was found before in [17].
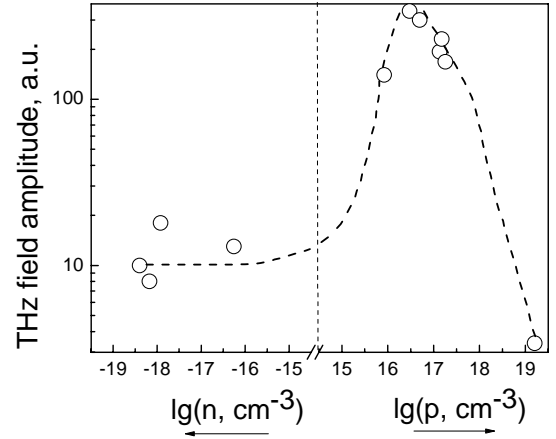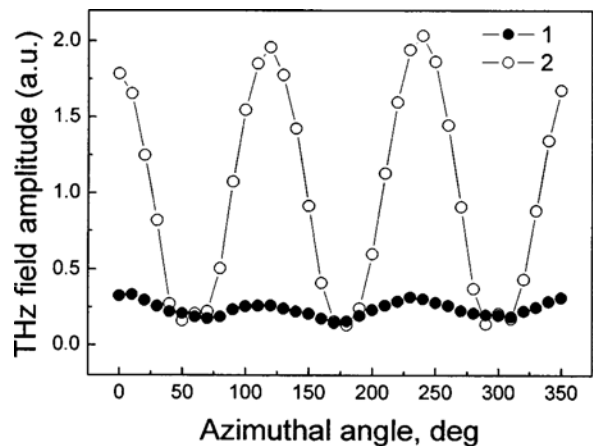

Fig.8. Azimuthal angle dependences of THz radiation emitted from the surfaces of two InAs samples with different doping levels: $n_0 = 10^{16}$ cm^{-3} (1) and $p_0 = 1.8 \cdot 10^{17}$ cm^{-3} (2).

Azimuthal angle dependence measurements are traditionally used for separating linear (photocurrent surge) and nonlinear (optical rectification) contributions to the THz radiation emission. For both traces shown on Fig. 8. THz field amplitude shows a clear periodicity of $\cos(3\theta)$ (θ is the azimuthal angle of the sample orientation around the axis normal to the surface) corresponding to the optical rectification effect at (111) surfaces. Such a periodicity in the (111) plane is characteristic for both bulk and electric-field-induced optical rectification [2,8], thus azimuthal angle dependencies alone cannot help by discriminating relative influences of these two effects. However, strong doping level dependence in p-InAs samples points out that, at least in this case, the prevailing physical mechanism of THz emission is the electric-field-induced instantaneous polarization. Surface depletion layer width in the samples with $p=10^{17}$ cm^{-3} is approximately the same as the light absorption length at the laser wavelength ($\sim$100 nm), therefore nonlinear optical interaction due to electric-field-induced optical rectification should be most efficient in this case.
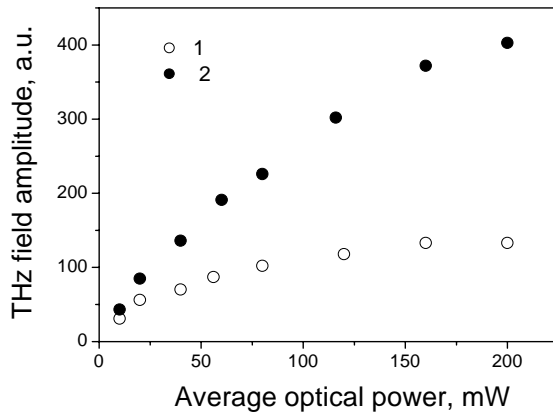

Fig. 9. Optical intensity dependences of the THz transient magnitudes measured at two azimuthal angles corresponding to the weakest (1) and the strongest (2) THz emission.

Relative role of this nonlinear optical process increases with increasing light intensity. This is illustrated by Fig. 9, where the intensity dependences of the THz transient magnitude measured at two azimuthal angles corresponding to the strongest and the weakest THz emission are shown. These dependences clearly show that the THz emission from p-InAs sample is caused by at least two different physical mechanisms. At low optical intensities where angular dependence of the radiated signal is weak, prevailing is, most probably, the current surge due to the transport of photoexcited carriers. With increasing intensity this effect is overpowered by the instantaneous polarization due to the electric-field-induced optical rectification. This conclusion is additionally supported by two additional experimental observations. First of all, the radiated THz transient magnitude saturates faster for the crystalline orientation corresponding to the minima of the angular dependence than to the maxima. The screening of the surface field that is most probable cause of this saturation would have a stronger influence on the carrier transport than on the nonlinear optical interaction, which will occur on a shorter time scale. Secondly, weak external magnetic field ($\sim$0.2

T) predominantly affects the THz field at azimuthal angles where nonlinear optical component is set to a minimum, where the component due to the photoexcited carrier transport that is prevailing (Fig. 10). Moreover, the polarities of the transients at two extrema of the angular dependencies are opposite, which is also consistent with the assumption of two different mechanisms of THz radiation.

3.1.2. Theoretical comparison of different mechanisms.

THz emission from semiconductor surfaces illuminated by femtosecond laser pulses is, in general case, caused by two effects: photocurrent surge at the surface and optical rectification due to the nonlinear difference frequency generation. Both these effects can be either independent on the surface electric field or linearly proportional to its strength. Photocurrent surge due to different diffusion rates for electrons and holes (the photo-Dember effect) and bulk optical rectification represent the first group of effects, whereas electron and hole separation by the surface field and electric-field induced optical rectification (EFIOR) – the second. It is generally assumed that the surface electric fields in narrow-gap semiconductors are weak due to their small energy bandgap, however, as it will be shown in the following, this is not always true, therefore one should consider all four physical mechanisms of THz generation.

In the dipole approach the electric field of THz pulse radiated by the laser illuminated semiconductor surface in the far field region is defined as

$$E(t) = -\frac{S}{c^2 R} \int_0^\infty (\frac{\partial j(z,t)}{\partial t} + \frac{\partial^2 P(z,t)}{\partial t^2}) dz \, , \tag{3}$$

where c is the light velocity in vacuum, R is the distance from the illuminated spot with the area S to the observation point, j and P are the photocurrent density and the polarization, z-axis is directed inward the sample. The first term in (3) is the current surge contribution and the second term is due to nonlinear optical rectification.

It is widely assumed that, for narrow-gap semiconductors, current surge contribution is dominated by the Dember effect and transient photocurrents caused by the surface field screening are much weaker. Monte Carlo simulations performed without taking into account the surface field show that the basic part of THz pulse in InAs, typical narrow-gap material, arises during the curse of first 100 – 200 fs after photoexcitation. THz generation is caused by asymmetric scattering of photoelectrons due to their reflection from the semiconductor surface. At this stage photoelectrons move ballistically (if their reflections from the surface are not taken into account). Solving the

17

kinetic equation for photoelectrons and the equation for electric field one can find the current density, which in the ballistic regime ($\omega_p \tau < 1$) is defined as

$$j(z,t) = \frac{e\alpha^2 W v_0 \exp(-\alpha z)}{3\hbar\omega\omega_p} e^{-t/\tau} \sin(\omega_p t) .$$ (4)

Here α is the absorption coefficient at the laser wavelength, W is the laser pulse fluence, $\hbar\omega$ is the photon energy, τ is the photoelectron momentum relaxation time, ω_p is the equilibrium electron plasma frequency, v_0 is the velocity of electron with energy of $\hbar\omega - \varepsilon_g$, and ε_g is the semiconductor bandgap. Substituting (4) in (3) one can obtain for THz field induced by the Dember effect

$$E_D(t) \approx \frac{e\alpha W v_0^2 S}{3c^2 R\hbar\omega} e^{-t/\tau} \cos(\omega_p t) .$$ (5)

The expressions (4) and (5) are obtained on the assumption that the excitation is instantaneous (laser pulse duration is zero), hence they can be used only for estimation purposes.

For InAs at 800 nm excitation, $v_0 = 1.5 \cdot 10^8$ cm/s, $\alpha = 7 \cdot 10^4$ cm^{-1}, $\hbar\omega = 2.95 \cdot 10^{-19}$ J. At the pulse energy WS=1 nJ and R=1 cm, the amplitude of THz field in free space is about 30 V/cm. As it follows from (3), the Dember-effect contribution to THz field grows quadratically with the increase of photoelectron velocity. The electric field oscillates with plasma frequency, which is defined by the equilibrium electron density; the contribution of photoelectrons in coherent plasma oscillation is suppressed due to nonparabolicity effect.

Nonlinear polarization P that is responsible for THz generation consists of two parts – intrinsic and electric field induced:

$$P_i = \chi_{ijk}(0,\omega,-\omega) E_j E_k^* + \chi_{ijkl}(0,\omega,-\omega,0) E_j E_k^* F ,$$ (6)

where χ_{ijk} and χ_{ijkl} are the second- and the third-order nonlinear susceptibilities, E is the optical field amplitude in the sample, F is the electric field at the semiconductor surface. In InAs having $\bar{4}3m$ symmetry the second-order susceptibility has only one nonzero component $\chi_2 = \chi_{x,yz}$, whereas the third-order susceptibility has three nonzero components $\chi_{x,xxx}, \chi_{x,xzz}, \chi_{x,zzx}$. THz electric field in the reflection direction is defined by the combination

$$(P_x \cos(\phi) + P_y \sin(\phi))\cos\theta + P_z \sin\theta \approx$$
$$-\chi_{xyz} E^2 \left(\sqrt{3} \sin\theta + \sqrt{\frac{2}{3}} \cos 3\phi \right) + FE^2 \left(3\chi_{x,xxx} \sin\theta - \frac{1}{\sqrt{2}}(\chi_{x,xxx} - \chi_{x,zzx} - 2\chi_{x,xzz})\cos 3\phi \right)$$ (7)

where ϕ is the azimuth angle between x-axis [11$\bar{2}$] direction) and the plane of incidence, θ is the refraction angle of THz radiation, z-axis is oriented in [111] direction inward the sample. On deriving (7) we used 45° angle of incidence of the laser beam and $\theta \approx 11^o$. One can see that both parts of the polarization in equation (7) include isotropic and azimuth-dependent contributions.

Let us estimate THz electric field induced by the optical rectification effect and compare it with the Dember-effect contribution (3):

$$E_{OR}(t) \approx \frac{8\pi S}{c^3 R} \frac{\partial^2}{\partial t^2} \left[\int_0^\infty (\chi_2 + \chi_3 F) I dz \right], \tag{8}$$

where $I(z,t) = \left(cE^2/8\pi \right)$ is the laser pulse intensity, χ_2 and χ_3 are the effective second- and third-order nonlinear susceptibilities. Within the linear approximation on excitation I, one can neglect the surface field screening caused by photocarriers. In this case, and by taking into account that $\partial^2 I/\partial t^2 \approx W/\tau_p^3$ (τ_p is the laser pulse duration), we obtain estimated amplitude of THz field as

$$E_{OR} \approx \frac{8\pi SW}{c^3 R \tau_p^3} \left[\int_0^\infty (\chi_2 + \chi_3 F(z)) e^{-\alpha z} dz \right] \approx \frac{8\pi SW}{c^3 R \tau_p^3 \alpha} (\chi_2 + \chi_3 F_{av}) \quad , \tag{9}$$

where F_{av} is the average surface electric field. The nonlinear susceptibility responsible for the second-harmonic generation in InAs is $\chi_2 \approx 10^{-6}$ CGSE. After substituting this value we obtain that the nonlinear optical rectification results in THz electric fields of about 0.03 V/cm, which is three orders lower than that for the Dember effect. At the fluences above 1 μJ/cm^2 the Dember contribution increases as logarithm and it is possible that the nonlinear effect compares with Dember effect and may be becomes dominant.

3.1.3. The effect of the surface modification

Additional proof of the role of the surface inversion layer was obtained from the investigation of the THz radiation emitted by InAs crystals with modified surfaces. This modification was performed either by surface sulfatization in the solution of $(NH_3)S_2$ or by sputtering a thin Mg layer on InAs surface. Sulfur passivation is known to increase surface band bending in InAs [27] and Mg is a shallow acceptor, thus it should lead the band flattening at p-InAs surfaces. One could expect that, *e.g.* for p-type InAs, sulfurization will increase the surface band bending, whereas the Mg-doping will lead to the flat band conditions. Fig. 10 illustrates the effect of surface modification by S and Mg doping on the azimuthal dependences of THz emission from p-type InAs crystals. As it has been expected, doping with sulfur increases the nonlinear optical component of THz emission, whereas Mg-doping nearly completely diminishes it. Experiments

evidencing the enhanced role of the optical rectification effect seemingly contradict the conclusion made before, when relative roles of the photo-Dember and the nonlinear optical effects were compared. It follows from this comparison that the magnitude of the latter effect should be small in InAs. This contradiction could be solved only by assuming that the nonlinear susceptibilities of InAs responsible for the optical rectification at the surfaces of InAs are much larger than the values used in Sect. 3.1.2.
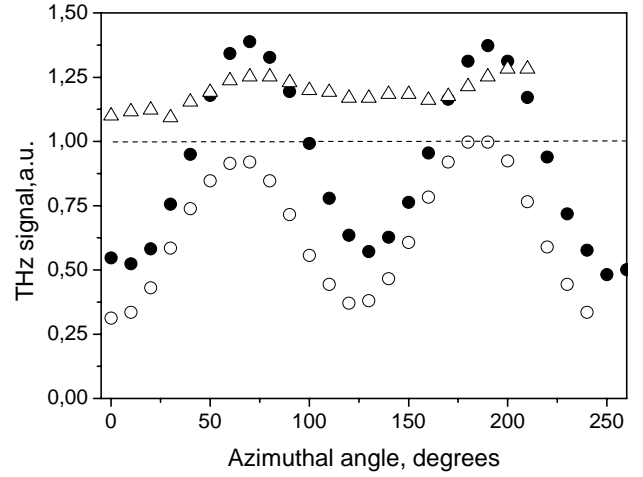
Fig. 10. The effect of InAs surface modification by sulfur (full circles) and magnesium (triangles) on azimuthal THz emission dependences. Empty circles show reference dependence measured on a freshly etched p-InAs surface.

3.2. THz emission spectroscopy of narrow gap semiconductors

Another question that remains unsolved yet is much weaker than in the case of InAs THz emission from another typical narrow gap semiconductor – InSb. Indium antimonide has a narrower bandgap, a smaller effective electron mass, and higher electron mobility than InAs, therefore one would expect it to be as efficient THz emitter as InAs. However, the THz power emitted from InSb illuminated by Ti:sapphire laser pulses ($\lambda \approx 800$ nm)surface is two orders of magnitude smaller than from InAs surface. One explanation of this contradiction could be the effect of the photoexcited electron scattering to subsidiary, high effective mass L valleys in the conduction band of InSb, where their mobility is much lower than in the main Γ valley [28]. In InAs the energy separation of Γ and L valleys is larger than in InSb [29], therefore the energy of the Ti:sapphire laser quantum is insufficient to start the intervalley transfer processes and the electrons remain in high mobility Γ valley. If these assumptions are correct, then a systematic study of the radiated THz power as a function of the laser wavelength could lead to a direct determination of the intervalley separation in the conduction band of a semiconductor, which is an important parameter for bandgap engineering of quantum confined structures based on narrow gap semiconductors.

In the present work, spectral dependences of the THz radiation from the laser-illuminated surfaces of InAs and InSb have been investigated experimentally for the laser wavelengths ranging from 0.6 μm to 2 μm. Clear maxima corresponding to the different spectral regions were observed and the intervalley separations for both materials were determined from the positions of these maxima.

Typical THz transient and its Fourrier spectrum are shown on Fig. 11. Fig. 12 presents the amplitudes of the THz signal radiated from InSb surface for different laser quantum energies. The values of the THz signal are normalized to the number of photons impinging the semiconductor at each laser wavelength. As it can be seen from this Figure, this dependence has a peak in the vicinity of ~0.77 eV. If one assumes that THz signal starts to decrease with increasing quantum energy $h\nu$ is the onset of the electron transfer to large effective mass L valleys, this value can be used for the determination of the intervalley separation in the conduction band $\Delta_{\Gamma L}$. The value of this parameter is equal to the electron excess energy ε_1 and could be found from the solution of the equations describing the energy and momentum conservation in the photon absorption process:
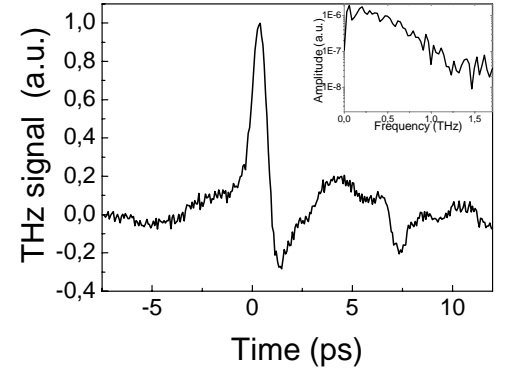

Fig. 11. The time-domain waveform measured on *n*-type InAs sample and its corresponding fast Fourier transform spectrum.
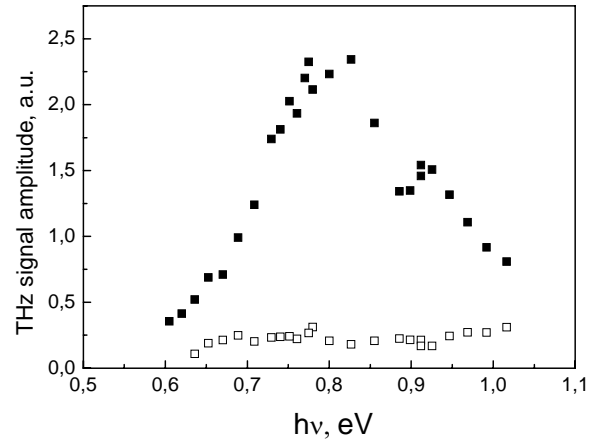

Fig. 12. THz signal radiated from InSb surface for different laser quantum energies and different azimuthal angles corresponding to minimum (open dots) and maximum (filled dots) signal amplitude.

$$\varepsilon_1 + \varepsilon_2 = h\nu - \varepsilon_g \tag{10}$$

$$\varepsilon_1(1 + \alpha\varepsilon_1)m_e = \varepsilon_2 m_{hh} \quad . \tag{11}$$

Here ε_2 is the excess energy of photoexcited heavy hole, ε_g is the energy bandgap, m_e and m_{hh} are the electron and heavy hole effective masses, and α is the coefficient for the nonparabolicity of the conduction band. By using InSb material parameters taken from [29] and listed on the Table I, one

could determine the intervalley separation for this semiconductor as $\Delta_{\Gamma L}$=0.53 eV. Similar procedure was applied to experimental results obtained on InAs and presented on Fig. 13. In this case, the intervalley separation in the conduction band of $\Delta_{\Gamma L}$=1.05 eV can be determined from the peak of the dependence corresponding to the photon energy of 1.6 eV. The values of $\Delta_{\Gamma L}$ evaluated in this work for both semiconductors are within the ranges set from the analysis of hot-electron and pressure dependent effects (0.45-0.65 eV for InSb and 0.8-1.1 eV for InAs [29]).

Table I. Parameters of the energy band structure of InSb and InAs [29].

Material	Bandgap energy, eV	Electron effective mass, m_0	Heavy hole effective mass, m_0	Nonparabolicity coefficient, eV^{-1}	Spin-orbital splitting, eV	Intervalley separation, eV (this work)
InSb	0.18	0.013	0.43	5.55	0.81	0.53
InAs	0.36	0.022	0.51	2.44	0.4	1.08

It has to be pointed out that the THz signal amplitude radiated from both semiconductors is strongly dependent on the azimuthal angle θ showing a unambiguous $cos(3\theta)$ dependences. Figs. 12 and 13 show spectral dependences of minima and maxima of these dependences. As it has been already demonstrated in [30] for highly excited InAs, the photo-Dember effect contribution is much smaller than the nonlinear optical effects. Three of such effects - bulk or surface electric field induced optical rectification
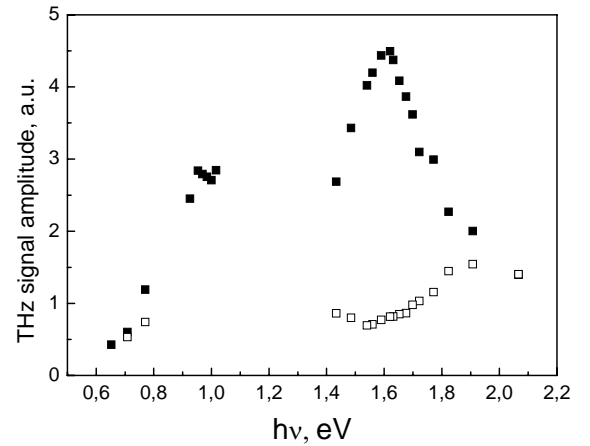

Fig. 13. THz signal radiated from InAs surface for different laser quantum energies and different azimuthal angles corresponding to minimum (open dots) and maximum (filled dots) signal amplitude.

and the shift current effect – have analogous azimuthal angle dependences, therefore cannot be distinguished by measuring these dependences. However, the shift current component, which depends on the free-electron scattering rate [30], will be affected by the onset of the intervalley scattering, therefore the measured spectral dependences evidence that this particular physical mechanism is responsible for the THz radiation from highly excited InAs and InSb.

For comparing different materials as prospective THz emitters, it is more convenient to plot their optical-to-THz power conversion efficiencies. Such plots for InSb and InAs are shown on Fig. 14. It can be seen from this Figure that in the near-IR range InSb is much better THz emitter than InAs. Moreover, the structure of the spectra is more complex than it could be envisaged from a simple model involving the onset of the intervalley transitions. For both InSb and InAs, maxima at ~1.3 μm additional to the ones explained by these transitions were
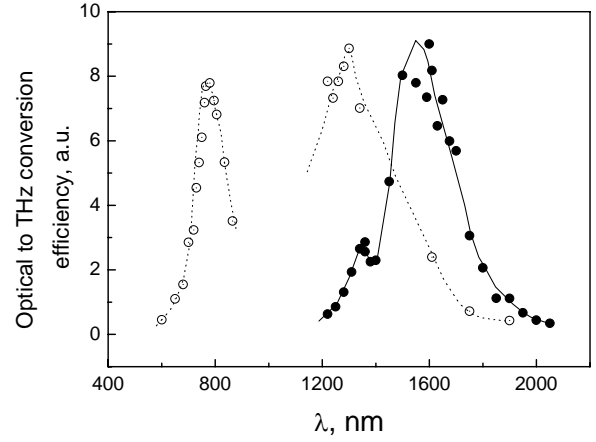
Fig. 14. Optical-to-THz power conversion efficiencies for InSb (full circles) and InAs (open circles).

observed. If in the case of InSb this additional maximum could be explained by the intervalley transitions of the electrons excited from the light-hole valence band, then for InAs the origin of the enhanced THz emission in this spectral range is unclear and requires a further investigation.

3.3. CdHgTe

Narrow gap semiconductors have high electron mobilities, which are thought to be one of the main reasons for their large THz emission efficiency. High electron mobility together with a large electron to hole mobility ratio results in a significant transient diffusion current at the surface due to the photo-Dember effect.
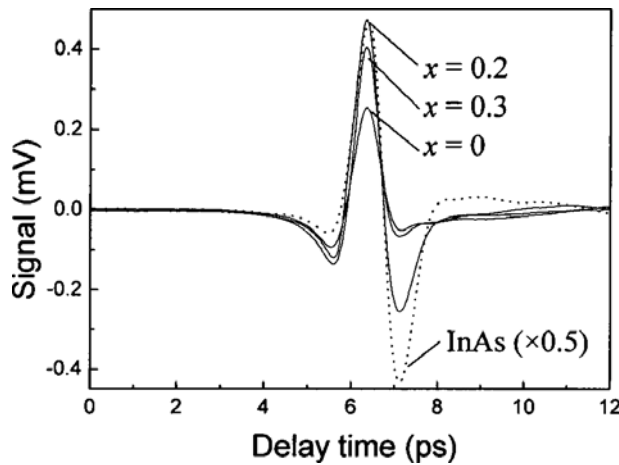
Fig. 15. THz field transients measured for the samples from different narrow-gap semiconductors.

However, InSb, another typical narrow gap semiconductor with an electron mobility almost twice as large as in InAs, is found to radiate a mere one hundredth of the THz power emitted by InAs. This discrepancy was explained by difference in the band structures of these materials at high electron energies and low-mobility conduction band valleys that are present in InSb at those energies. The goal of the work described in the present chapter was to investigate THz radiation from

Cd$_x$Hg$_{1-x}$Te crystals, narrow gap semiconductor compounds that are widely used in infrared devices. By changing the alloy composition of Cd$_x$Hg$_{1-x}$Te, a large variety of different band structures can be realized, therefore it can be expected that such an investigation could lead to a discovery of the materials with properties suitable for THz emission.

Fig. 15 shows the time-domain waveforms measured on InAs and three Cd$_x$Hg$_{1-x}$Te samples with different alloy composition. In this experiment, the emitting semiconductor samples were placed in proximity (at ~5 mm distance) to the silicon dome focusing THz radiation on the detector. Peak field values in the majority of THz transients measured on Cd$_x$Hg$_{1-x}$Te samples are only 2-3 times smaller than in InAs, however in the later case positive peak is followed by a negative dip of nearly the same magnitude leading to much larger enhancement of the emitted THz power.
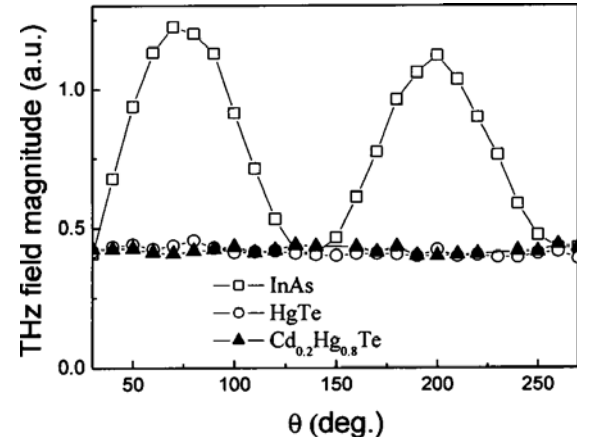

Fig.16. Azimuthal angle dependences of THz field magnitude emitted from the surfaces of different narrow-gap semiconductors.

Fig. 16 presents the results of the azimuthal angle dependence measurements of THz transient magnitude. Such measurements are traditionally used for separating linear (photocurrent surge) and nonlinear (optical rectification) contributions to the THz radiation emission. For a reference InAs sample THz field amplitude shows a clear periodicity of cos(3θ) (θ is the azimuthal angle of the sample orientation around the axis normal to the surface) corresponding to the optical rectification effect at (111) surfaces. Nonlinear, angle dependent contribution to the total THz radiation is approximately 40 %, which corresponds to the data obtained in an earlier investigation of n-InAs [17]. On the other hand, the magnitude of the THz field radiated from both HgTe and Cd$_{0.2}$Hg$_{0.8}$Te (100) surfaces does not depend on the azimuthal angle of sample orientation, which can be considered as an evidence of a prevailing role of linear processes in THz radiation from these materials.

The fact that THz emission from the surfaces of Cd$_x$Hg$_{1-x}$Te crystals is caused by fast changing photocurrent is also confirmed by the experiment on the magnetic field influence on the shape of the transients. The results of this experiment for one of the samples (Cd$_{0.2}$Hg$_{0.8}$Te) are shown in Fig. 17. Relatively week (B=0.28 T) field of a permanent magnet parallel to the illuminated surface of the sample leads, depending on its polarity, to the increase or the decrease of THz transient magnitude. This observation is consistent with the model explaining the magnetic field influence by the Lorentz-force induced rotation of the radiating dipole orientation [32].

Fast changing photocurrent at semiconductor surface can originate from two physical effects: the acceleration of photoexcited carriers by th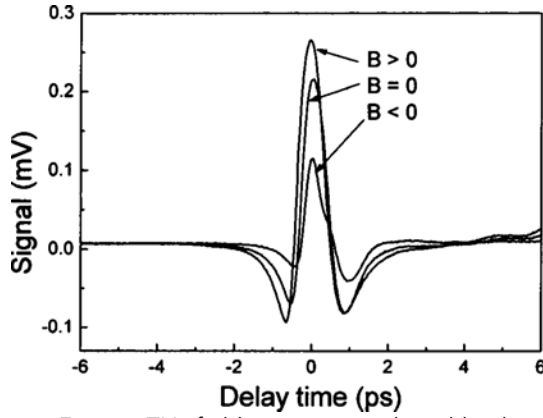e built-in field in the surface depletion layer or the photo-Dember effect caused by the different electron and hole diffusion rates. In $Cd_xHg_{1-x}Te$ the surface field will be weak because of a small energy band gap, whereas the carrier diffusion processes will be rather intense due to short light absorption lengths. Consequently, the ultrafast photocurrent transients due to the photo-Dember effect may be the main mechanism of THz radiation emission from these semiconductors.

Fig.17. THz field transients radiated by the sample of $Cd_{0.2}Hg_{0.8}Te$ without and with magnetic field (B=0.28 T) of two opposite polarities.

According to the formula (1) for the photo-Dember voltage, the THz field magnitude should be proportional to the photoexcited electron excess energy, which leads to interesting conclusions regarding the energy band structure of $Cd_xHg_{1-x}Te$ alloys.

Band structure of this alloy system changes drastically when altering the alloy composition [31]. This is illustrated in Fig. 18 where band lineups at the center of the Brillouin zone (point Γ) for three alloy compositions investigated in the present work are shown schematically. On substituting Cd for the heavy Hg atom the energy spectrum of the $Cd_xHg_{1-x}Te$ alloys exhibits a transition from a semimetal behavior in HgTe to a semiconductor behavior in CdTe. The bandgap changes almost linearly with x and becomes equal to ε_g= 0.35 eV for x= 0.3. Spin-orbital split band Γ_7 energetic position relative to the heavy hole band is changin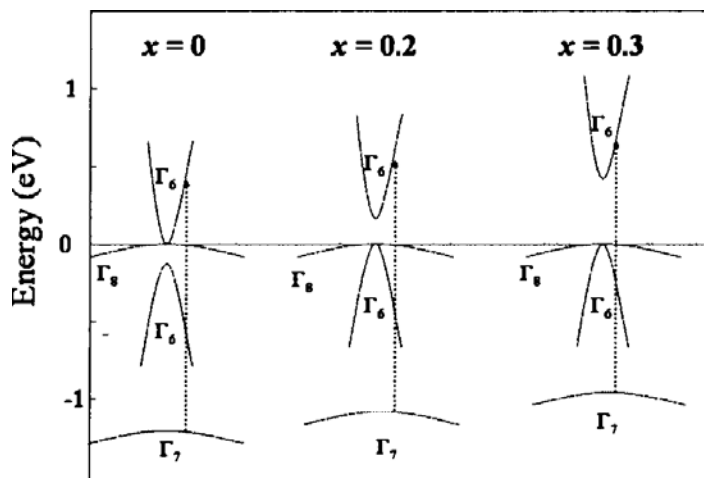g with the alloy composition slower than the bandgap and, for the alloy compositions investigated in our work, is in the range of Δ_0= 1-1.2 eV.

Fig.18. Schematic band structures of various $Cd_xHg_{1-x}Te$ alloys.

Optical pulses generated by Ti:sapphire laser (hv= 1.51 eV) can excite electrons from all three: light-hole, heavy-hole, and spin-orbital split valence bands. Excess energy of electrons and THz transient magnitude excited by first two of those transitions will decrease with x, which is

inconsistent with the experimental observations. Moreover, transitions from the heavy-hole band will excite electrons to very high energies in the conduction band, where their scattering to the subsidiary, larger effective mass L-valleys (positioned at 1.2-1.4 eV in CdTe-HgTe system [31]) reducing the photo-Dember voltage is possible. Therefore, we suppose that most important are the transitions from the spin-orbital split valence band to Γ_6 conduction band valley. Arrows on Fig. 18 indicate these transitions.

3.4 Germanium

3.3.1. Experimental investigation of THz emission

The data on THz emission from the surfaces of elementary semiconductors are scarce. In silicon only a weak emission due to the instantaneous polarization due to the photoexcitation of the externally biased crystal was documented [33], whereas Ge was only shortly mentioned among the semiconductor materials exhibiting a weak THz emission in [2]. In this chapter we present a more systematic study of THz radiation emitted by femtosecond laser excited Ge crystals. Results obtained by investigating differently doped samples were compared and the conclusions regarding the physical mechanism leading to the THz emission from these crystals are drawn.

Fig. 19 shows the time-domain waveforms measured on several n-type Ge samples with different electron concentrations and their corresponding fast-Fourier transform spectra.

Fig 19. The time-domain waveforms measured on several *n*-type Ge samples with different electron concentrations (a) and their corresponding fast-Fourier transform spectra (b). By vertical lines are indicated calculated plasma frequencies for some samples.

Similar results obtained on several p-Ge samples are presented in Fig. 20. Transients obtained on n-Ge samples are of a larger magnitude than those measured on p-Ge samples, but even the largest THz transient radiated from n-Ge surface was approximately 5 times smaller than the signal radiated by p-InAs surface under the same conditions. One has to point out that the transients radiated by both n-type and p-type Ge surfaces are of the same polarity, their magnitude increases
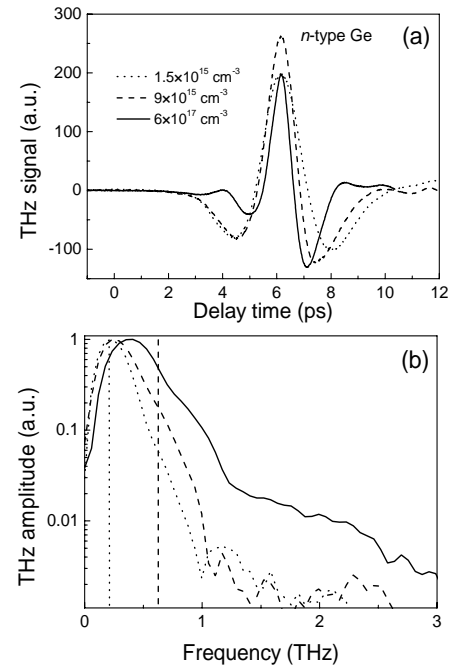
linearly with increasing optical power and reaches maximum at n~10^{17} cm^{-3} and p~10^{16} cm^{-3}, respectively.

Fourier spectra of the data are shown in Fig. 19b and Fig. 20b. They reveal for all doping concentrations distinctive amplitude spectra. Frequencies corresponding to the peak signal magnitudes for all the spectra increase with increasing doping level of the samples. Such peak frequency dependence on the equilibrium carrier concentration is usually considered as a proof of the cold-plasma oscillation mechanism of the THz emission [34]. By vertical lines on Fig. 19b and Fig. 20b, together with experimentally obtained THz emission spectra are indicated plasma frequencies for respective samples calculated by using a simple formula (3).

As it can be seen from these Figures, the calculated plasma frequencies coincide with the maxima positions on the experimental spectra only for the samples with the lowest electron or hole concentrations; for larger carrier densities the theoretically predicted plasma frequencies are higher than the observed experimentally. This discrepancy can be explained by the limited temporal resolution of our THz detection system based on LTG GaAs photoconducting antenna.

Fig 20. The time-domain waveforms measured on several *p*-type Ge samples with different holes concentrations (a) and their corresponding fast-Fourier transform spectra (b). By vertical lines are indicated calculated plasma frequencies for some samples.

In n-GaAs, where THz emission caused by a similar effect – cold plasma oscillation has been documented [32], this oscillation was initiated by photoexcited current surge in the built-in field at the surface of the crystal. In the case of THz emission from Ge surface illuminated by femtosecond laser pulses this mechanism is less likely. The surface electric fields in n-Ge and p-Ge crystals have opposite polarities [35], therefore of opposite polarity should be also the THz transients radiated by those crystals. However, the experiments evidence that the signs of THz transients emitted by n and p-Ge surfaces are the same, which means that the photocurrent surge in the built-in surface field is not responsible for the excitation of the plasma oscillation.
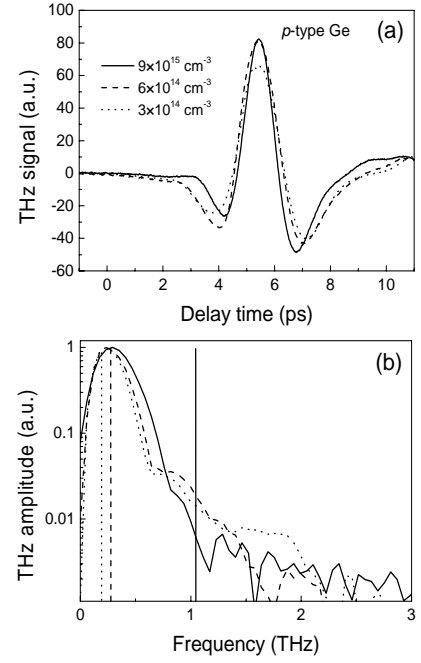
3.3.2. Optical pump – THz probe experiment

As an alternative mechanism of the plasma oscillation excitation we consider the photo-Dember effect caused by different diffusion speed of the electrons and holes created at the surface of the crystal by the laser pulse. Such a mechanism of THz radiation was evidenced before in the case of InAs crystals [17]. In InAs case, electrons are more mobile than the holes, therefore immediately after the excitation they move further down from the surface as the holes, thus creating a transient electrical polarization. For both n- and p-type Ge samples the polarity of the radiated THz transient also corresponds to the situation with electrons more mobile than the holes. Electrical transport dynamics in these samples on the subpicosecond time scale was investigated in a separate experiment.
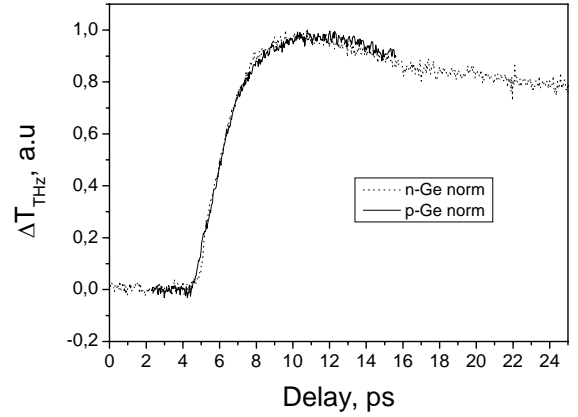

Fig. 21. The temporal dynamics of optical pump induced change in the transmittance at THz frequencies obtained on both *n* (dotted line) and *p*-type (solid line) Ge samples.

For this experiment optical pump – THz probe technique was employed. Both THz radiation pulse emitter and detector were made as dipole antennae on LTG GaAs layer and were activated by the parts of Ti:sapphire laser beam. The third part of the same laser beam was used for the photoexcitation of the samples. The samples of n- and p-type Ge with the highest resistivity available (ρ=10 Ωcm) were placed right behind the metallic aperture with the diameter of 300 μm; both optical pump and THz probe beams were made overlap at this aperture. The dependence of the THz transient signal at its maximum was measured at different delays of the optical pump pulse. The temporal resolution of this experiment was determined by the response of the detector measuring THz transients and was approximately equal to 500 fs.
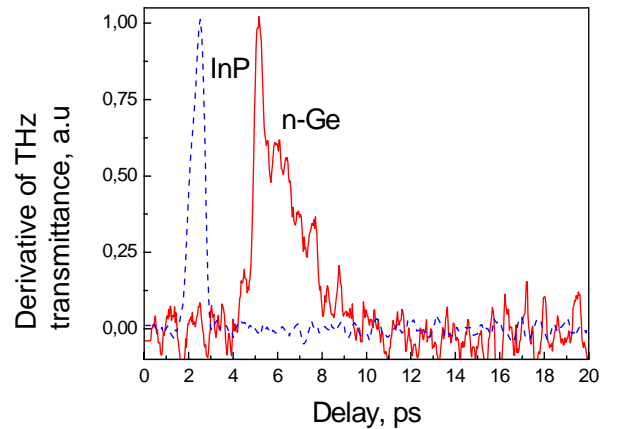

Fig. 22 Time derivatives of the rising parts of typical THz transmittance transients measured on InP (dashed line) and *n*-type Ge (solid line).

Fig. 21 shows the temporal dynamics of optical pump induced change in the transmittance at THz frequencies measured by this technique. Experimental traces obtained on both n and p-type Ge samples coincide with each other within the experimental accuracy. It should be noted that the rise time of the induced THz transmittance transient is unexpectedly long – several picoseconds. Similar transients when measured on such direct bandgap semiconductors as InP or GaAs usually were characterized by the rise times comparable with the temporal resolution of the experiment (~0.5 ps). The differences between Ge and direct bandgap semiconductors become even more striking when one compares time derivatives of the rising parts of typical THz transmittance transients measured on these materials (Fig. 22). It is clearly seen from Fig. 18 that the rise time of the transient measured on germanium crystal consists of two parts: a fast changing part with duration of ~0.7 ps, which is also typical for InP, and a slower changing rise of the induced transmittance (characteristic time of ~ 2 ps).

Experiments described above allow us to get an insight on the physical mechanisms leading to the emission of THz radiation at the surfaces of Ge crystals after their illumination by femtosecond laser pulses. The polarity of THz electrical transients is the same for n-type and p-type Ge surfaces, which suggests that the photoinjected carriers lead to the build-up of the Dember field due to the diffusion current associated with the generated electrons and holes. This field causes the restoring force of the carrier motion and thus starts oscillating motion of the charge carriers. THz spectra radiated by differently doped Ge samples shift to the higher frequencies with increasing doping density, evidencing that this oscillation involves mainly the "cold" plasma consisting of equilibrium electrons and holes. Photoexcitation of germanium by Ti:sapphire laser pulses in a nontrivial process. It is, *e.g.*, not evident which kind of the photoexited carriers: electrons or holes are more mobile during the first few hundreds of femtoseconds, when the THz transients are generated. Experimentally determined polarities of these transients suggests that the electron diffusion is faster than the hole diffusion. On the other hand, the energy quanta of Ti:sapphire laser are much larger than the energy bandgap of Ge, therefore optically excited electrons should have large excess energies and could be transferred to conduction band valleys with low electron mobilities. Optical pump – THz probe experiments that have been performed in the present work facilitate a better understanding of these transport processes occurring right after the photoexcitation of the sample. Light induced change in the THz transmittance, which is the measure of the photoexcited conductivity in the sample, was measured in these experiments. For a better understanding of the processes determining the electron transport on the subpicosecond time scale it is worth to analyse the electronic band structure of germanium, which is schematically shown on Fig. 23. Lowest energy minima in the conduction band of this material are at L points of the Brillouen zone.
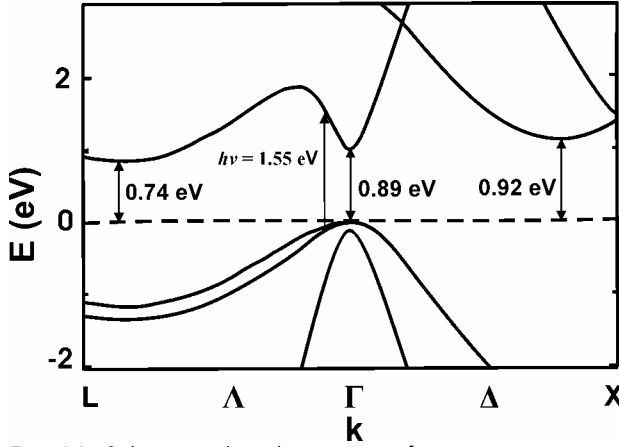
Fig. 23. Schematic band structure of germanium.

Because the energy bandgap of Ge is only ~0.9 eV, Ti:sapphire laser quanta (hν=1.55 eV) are exciting electrons high into the energy states of the central Γ minimum. These states are higher than the energy position of Δ-minima – another group of non-equivalent valleys in Ge lying at ~0.18 eV above the main L minima. Electron-optical phonon interaction in Γ-valley is forbidden due to symmetry considerations, therefore the main scattering mechanisms are intravalley acoustic phonon and intervalley transitions. Both Γ-L and Γ-Δ intervalley transitions are possible. These transitions lead to a redistribution of the electrons between different groups of valleys even during the laser pulse. Using the energy band parameters of Ge from Ref. 36 the ratio of the density of states in the L, Δ, and Γ can be found as 1:2.7:0.02; therefore more than 70% of all photoexcited electrons will be transferred to subsidiary Δ-valleys. Electron mobility in Δ-valleys is ~10 times lower than in the lowest lying L-valleys [37], therefore the contribution of Δ-valleys to THz wave absorption is negligible. As a consequence, transient THz transmittance will reach approximately 30% of its magnitude during the action of the laser pulse; further increase of the induced transmittance is associated with the cooling of the electrons in Δ-valleys and their transfer to the higher mobility L-valleys. The characteristic duration of the later process will be comparable with the hot-electron energy relaxation time in germanium, which at room temperature is of the order of several picoseconds [38].

3.3.3. Model calculations and discussion of the results.

In the present work an ensemble Monte Carlo method is used to study photo-Dember effect and terahertz (THz) pulses generation in Ge excited by femtosecond laser irradiation. In our calculation Herring and Vogt transformation [36, 39] was used for the electrons in the L valleys, turning the ellipsoidal constant energy surfaces of those valleys spherical. The contribution of Δ - electrons to THz transient generation is rather small due to their low mobility, therefore a simplified, spherically symmetric model of the Δ-valleys was assumed in the calculation. In the valence band of germanium only the heavy holes with an isotropic dispersion law is taken into account. The intra-valley scattering of electrons and holes in Ge are assumed to interact with acoustic and optical phonons. Deformation potential type interaction was taken into account;

electrons in Γ and Δ valleys did interact only with the acoustic phonons. Intense inter-valley scattering which results in the transfers of electrons between equivalent and non-equivalent valleys of the conduction band was also taken into account in our Monte Carlo procedure similarly as it has been done in [36].

The electric field caused by the spatial separation of photoexcited electrons and holes was determined self-consistently from one-dimensional Poisson equation that was solved numerically with using the finite-difference method on the grid with the spatial step of 0.002 μm. The simulations were carried out for n-and p-type Ge ($1.5 \cdot 10^{15}$ cm^{-3}) samples excited by 150 fs duration laser pulse with 1.55 eV photon energy. An ensemble of 50 000 macroparticles was used; the electric field was recalculated with a time step of 2 fs. The electric field at the surface of semiconductor is supposed to be lacking that is the Fermi-level pinning is ignored. The effective masses of electrons and holes, valley separations, the intra-valley and inter-valley deformation potentials, and the energy of the optical and inter-valley phonons for Ge are taken from [40]. The optical absorption and reflection coefficients at the wavelength of about 800 nm are chosen to be 5 10^4 cm^{-1}and 0.42 accordingly [40].

Experiments described above allow us to get an insight on the physical mechanisms leading to the emission of THz radiation at the surfaces of Ge crystals after their illumination by femtosecond laser pulses. The polarity of THz electrical transients is the same for n-type and p-type Ge surfaces, which suggests that the photoinjected carriers lead to the build-up of the Dember field due to the diffusion current associated with the generated electrons and holes. This field causes the restoring force of the carrier motion and thus starts oscillating motion of the charge carriers. THz spectra radiated by differently doped Ge samples shift to the higher frequencies with increasing doping density, evidencing that this oscillation involves mainly the "cold" plasma consisting of equilibrium electrons and holes.
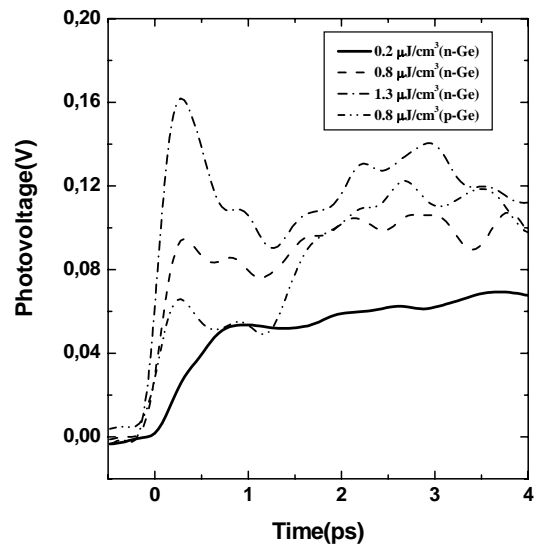

Fig. 24. The calculated temporal dependencies of the Dember photovoltage in n- and p-Ge excited by 150 fs laser pulse under different excitation fluences

The calculated temporal dependencies of the Dember photovoltage in n- and p-Ge excited by 150 fs laser pulse under different excitation fluences are shown in Fig. 24. The excitation level of 0.8 $\mu J/cm^2$ corresponds to photoexcited electron-hole pair density at the surface of Ge of $9 \cdot 10^{16} cm^{-3}$. As one can see, for about 100 fs after the photoexcitation, the surface photovoltage grows abruptly and, after having gone through a minimum, reaches maximum value at a time of about 3 ps. Simulations show that electrons generated initially in the central valley are transferred to the lower lying L and Δ valleys in ~ 50 fs (Fig. 25). Electrons populating these valleys have high excess energy (~ 0.5 eV) and for a time duration of about 100 fs move quasi-ballistically with a high velocity leaving behind the holes. After a few scattering events electrons lose their excess energy and their transport becomes dominated by the diffusion. Since at this stage most of the electrons still populate Δ valleys, where their mobility is lower than the mobility of the holes and the in L-valley electrons, the holes catch up with the electrons and the photovoltage starts to decrease.

At a later stage of the photoexcited electron dynamics, the population of the Δ valleys starts to cool down and the electrons are transferred to L valleys, therefore average electron mobility becomes larger than the hole mobility and surface photovoltage begins to rise again. As it can be seen from the results of the modelling (Fig. 25), Δ-L transfer time is about 3 ps, which is close to the value obtained from the optical pump – THz probe experiment. Subsequently, the photovoltage begins to decrease and approach its typical quasi-equilibrium value. At this stage the Dember electric field accelerates the holes and slows
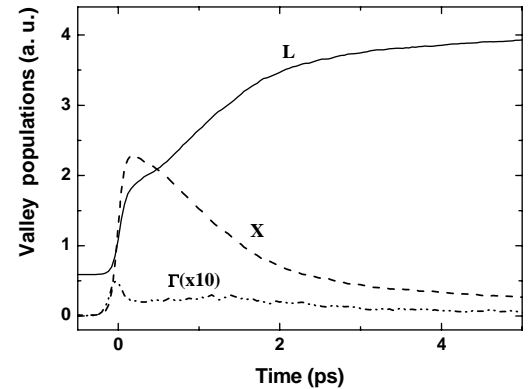

Fig. 25. The simulated kinetics of photoexcited electron population in Γ, Δ, and L valleys.

down the electrons, therefore electrons and holes move with the same velocities as a quasi-neutral cloud (ambipolar diffusion regime). It should be pointed out that under femtosecond laser excitation the surface photovoltage in Ge is several times larger than the quasi-stationary Dember photovoltage. This enhancement can be explained in terms of hot carrier diffusion and quasi-ballistic transport that prevail at initial moments after excitation.

Average partial currents of holes and electrons from the different valleys calculated for n-Ge photoexcited at 1.3 μJ/cm^2 fluence are presented in Fig.26. Simulations show that the contribution to the current of the central Γ-valley electrons is negligible (not shown in Fig. 26), because they are transferred to the lateral valleys, mainly to the Δ-valleys, very fast. Partial current of Δ-valley electrons reaches its maximum value at about 100 fs after photoexcitation; however this value is 4 times lower than the current produced by L-valley electrons. It can also be seen from Fig. 26 that at the initial stage, when electrons and holes move ballisticaly, the electron current increases faster than the hole current indicating that the ballistic movement of photoexcited electrons dominates over that of the holes. At about 0.3 ps after the photoexcitation the total current changes its sign as a result of increasing hole contribution; at the later stages hole and electron currents equilibrate each other, which leads to an ambipolar diffusion of the carriers. It should to be pointed out that the establishment of this regime can proceed in time either
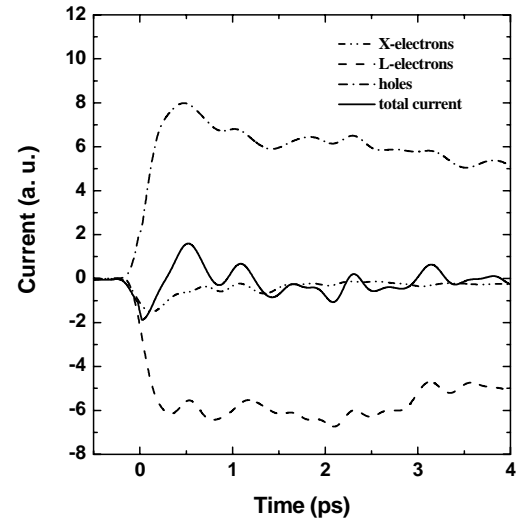

Fig. 26. Average partial currents of holes and electrons from the different valleys calculated for *n*-Ge photoexcited at 1.3 μJ/cm² fluence.

monotonically or oscillatory with plasma frequency. The simulations indicate that the oscillatory behavior of the photovoltage and current takes place at high excitation level (Fig. 24 and Fig. 26).

Temporal waveforms of the emitted THz pulses can be found by differentiating of the total current over time (Fig. 27). It can be seen from that Figure that the peak of THz transients correspond to the stage where ultrafast ballistic transport of photocarriers is prevailing. Calculated duration of the THz pulse turns out to be slightly shorter than the experimentally observed pulse duration, most probably due to limited temporal resolution THz detection system used in the experiments.

Monte Carlo modeling was also be used for interpreting the results of the optical pump – THz probe measurements. Comparison between the theory and the experiments are shown on Fig. 28. Calculated transients are convoluted with 500-fs long (FWHM) probe pulses. Three values of the coupling constant with acoustic phonons responsible for L-Δ intervalley scattering were used in the calculation; the best agreement between the theory and the experiment was achieved for the

coupling constant equal to $4 \cdot 10^8$ eV/cm. It has to be pointed out that this value coincides with the coupling constant that was used in [36] for the description of the hot-electron negative-differential-mobility effect in germanium.

The laser pulse duration in our experiments was longer than 50 fs, at which the photoexcited electrons from Γ valley are scattered to L and Δ valleys; therefore Γ valley contribution to the electrical transport effects was rather weak. The situation could be completely different when shorter laser pulses would be used for the excitation of Ge surfaces. In such a case, electron intervalley scattering could act as an additional photocurrent decay

Fig. 27. Calculated temporal waveforms of the emitted THz pulses.

mechanism leading to extremely fast current transients. These transients could be successfully exploited in laser-activated dipole antennae for THz radiation generation and detection as well as in
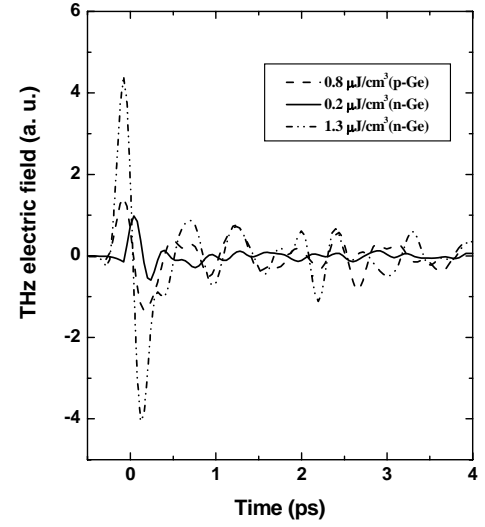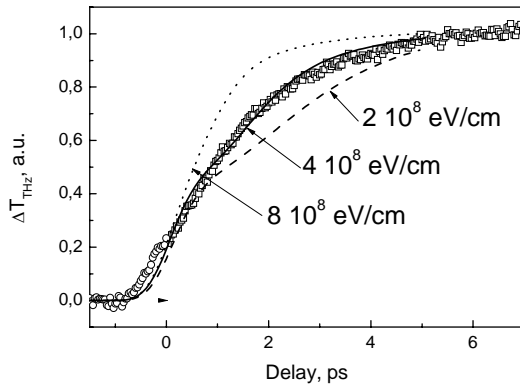

Fig. 28. The initial part of the temporal dynamics of optical pump induced change in the transmittance at THz frequencies obtained on p-type Ge sample (open circles). Dots, solid line, and dashed line correspond to the Monte Carlo simulations with different intervalley coupling constants.
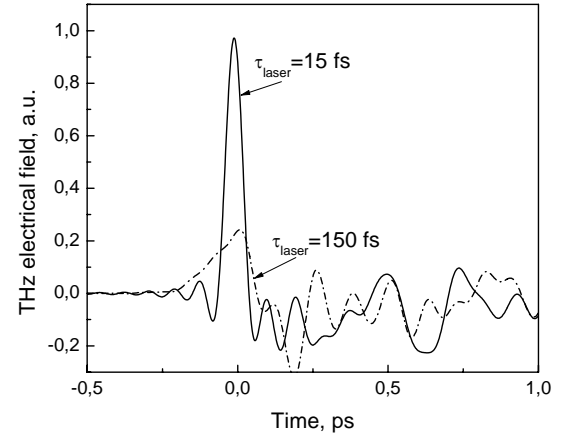

Fig. 29. Calculated temporal waveforms of THz signals emitted from the Ge surfaces excited by 150 fs and 15 fs duration pulses.

wide-band surface emitters at THz frequencies. It is known, *e.g.*, that Ge surfaces illuminated by 100-fs and longer laser pulses are rather poor THz radiation emitters [2], however, when excited by much shorter laser pulses, the use could be made from the very fast ballistic movement of the electrons in the low effective mass G valley and the enhancement of the photocurrent surge at the illuminated surfaces. Fig. 29 compares simulated THz

transients radiated by the Ge surfaces excited by 150 fs and 15 fs duration laser pulses. As it can be seen from this Figure, the shortening of the pulse duration increases the THz transient amplitude by nearly one order of magnitude making Ge comparable to the best surface emitter materials.

4. Conclusions

In conclusion, we have investigated THz emission from laser irradiated surfaces of several narrow gap semiconducting materials.

Most efficient emitter when 700-800 nm wavelength (corresponding to the spectral range of Ti:sapphire laers) pulses are used for the photoexcitation is InAs; in the 1.4-1.8 μm spectral range optical to THz power conversion efficiency is the largest for InSb.

Both the photo-Dember effect and the shift current contribute to the THz signal radiated from InAs surface; relative importance of these physical mechanisms varies with varying laser irradiation.

THz emission from laser illuminated surfaces of CdHgTe is determined by the photo-Dember mechanism and is weaker than the emission from $A_{III}B_V$ narrow gap semiconductor compounds.

The effect of THz emission from the semiconductor surfaces can be successfully employed for determining parameters of photoexcited materials; good examples of such application are the determination of the intervalley energy separation in the conduction bands of InAs and InSb as well as the findings related to the deformation potential for electron intervalley scattering in germanium.

References

1. D. Krokel, D. Grischkowsky, M. B. Ketchen, *Appl. Phys. Lett,.* **54**, 1046 (1989).

2. X.-C. Zhang and D. H. Auston, *J. Appl. Phys.* **71**, 326 (1992).

3. Q. Wu , X.-C. Zhang, *Appl. Phys. Lett.*, **56**, 886 (1990).

4. P. N. Saeta, B. I. Greene, S. L. Chuang, *Appl. Phys. Lett.*, **63,** 3482 (1994).

5. A. Rice, Y. Jin, X. F. Ma, X.-C. Zhang, D. Bliss, J. Larkin, and M. Alexander, *Appl.Phys.Lett.*, **64**, 1324 (1994).

6. J. E. Sipe and A. I. Shkrebtii, *Phys. Rev*. B **6**1, 5337 (2000).

7. D. Cote, N. Laman, and H. M. van Driel, *Appl.Phys. Lett.*, **80** , 905 (2002).

8. S.L. Chuang, S. Schmitt-Rink, B.I. Greene, P.N. Saeta, and A.J. Levi, *Phys. Rev. Lett.*, **68,** 102 (1992).

9. M. Nakajima,Y. Oda, and T. Suemoto, *Appl. Phys. Lett*., **85,** 2594 (2004).

10. R. Ascazubi, I. Wilke, K. Denniston, Hai Lu, and W. J. Schaff, *Appl. Phys. Lett*., **84**, 4810 (2004).

11. J. Shan, C. Weiss, R. Wallenstein, R. Beigang, and T. F. Heinz, *Opt. Lett*. **26**, 849 (2001).

12. N. Sarukura, H. Ohtake, S. Izumida, and Z. Liu, *Appl. Phys. Lett*. **84**, 654 (1998).

13. S. Kono, P. Gu, M. Tani, and K. Sakai, *Appl. Phys. B: Lasers Opt*. 901 (2000).

14. M. Zedler, C. Janke, P. Haring Bolivar, H. Kurz, and H. Kuenzel, *Appl. Phys. Lett.*, **83**, 4196 (2003).

15. T. Dekorsy, H. Auer, C. Waschke, H. J. Baker, H. G. Roskos, H. Kurz, V. Wagner, and P. Grosse, *Phys. Rev. Lett.,* **74,** 738 (1995).

16. H. Dember, Phys. Z. **32**, 554 (1931).

17. P. Gu, M. Tani, S. Kono, K. Sakai, and X-C. Zhang, *J. Appl. Phys*., **91**, 5533 (2002).

18. W. Sha, A. L. Smirl, and W. F. Tseng, *Phys. Rev. Lett*. **74**, 4273 (1995).

19. M. Vossebuerger, H. G. Roskos, F. Wolter, C. Waschke, H. Kurz, K. Hirakawa, I. Wilke, and K. Yamanaka, *J. Opt. Soc. Am. B* **13**, 1045 (1996).

20. R. Kersting, J. N. Heyman, G. Strasser, and K. Unterrainer, *Phys. Rev.,* **58B**, 4553 (1998).

21. Kai Liu, A Krotkus, K. Bertulis, Jingzhou Xu, and X.-C. Zhang, *J. Appl. Phys*, **94**, 3461 (2003).

22. A. V. Kuznetsov and C. J. Stanton, *Phys. Rev.* B **48**, 10 828 (1993).

23. M. Tani, R. Fukasawa, H. Abe, S. Matsukura, K. Sakai, and S. Nakashima, *J. Appl. Phys.*, **83,** 2473 (1998).

24. J. N. Heyman, P. Neocleous, D. Hebert, P . A. Crowell, T. Mueller, and K. Unterrainer, *Phys. Rev.* B **64**, 085202 (2001).

25. H. Takahashi, M. P. Hasselbeck, A. Quema, M. Goto, S. Ono, and N. Sarukura, *Jap. J. Appl. Phys.,* **43**, L221 (2004).

26. M. P. Hasselbeck, D. Stalnaker, L. A. Schlie, T. J. Rotter, A. Stintz, and M. Sheik-Bahae, *Phys. Rev. B* **65**, 233203 (2002).

27. D.Y. Petrovykh, M.J. Yang, and L.J. Whitman, *Surf. Sc.*, **523**, 231-240 (2003).

28. S. C. Howells, S. D. Herrera, and L. A. Schlie, Appl. Phys. Lett., **65**, 2946 (1994).

29. A. Krotkus and Z. Dobrovolskis, *"Electrical conductivity of narrow-gap semiconductors"*, Mintis, Vilnius, 1988.

30. M. Reid and R. Fedosejevs, Appl. Phys. Lett., **86**, 011906 (2005).

31. R. Dornhaus, G. Nimtz, and B. Schlicht, *Narrow-gap Semiconductors* (Springer-Verlag, Berlin, 1983).

32. M. B. Johnston, D. M. Whittaker, A. Corchia, A. G. Davies, and E. H.Linfield, *Phys. Rev.* B **65**, 165301 (2002).

33. B. B. Hu, E. A. Souza, W. H. Knox, J. E. Cunningham, M. C.Nuss, A. V. Kuznetzov, and S. L. Chuang, *Phys. Rev. Lett.* **74**, 1689 (1995).

34. R. Kersting, J. N. Heyman, G. Strasser and K. Unterrainer, *Phys. Rev. B*, **58**, 4553 (1998).

35. J. A. Dillon and H. E. Farnsworth, *J. Appl. Phys.,* **28**, 174 (1957).

36. W. Fawcett and E.G.S. Paige, *J.Phys.* C, **4**, 1801 (1971).

37. K. Fletcher and G. D. Pitt, *J.Phys.* C, **4**, 1822 (1971).

38. V. Dienys, Z. Kancleris, Z. Martunas, „Warm electrons", Mokslas, Vilnius, 1983.

39. C. Jacoboni and L.Reggiani, *Rev. Mod. Phys.*, **55**, 645(1983).

40. A.Dargys, J. Kundrotas, *Handbook on Physical Properties of Ge, Si, GaAs and InP* (Science and Encyclopedia Publishers, Vilnius, 1994).

Articles with the acknowledgement to US Air Force EOARD

1. **R. Adomavičius,, A. Urbanowicz, G. Molis, A. Krotkus, E. Shatkovskis,** "Terahertz emission from *p*-InAs due to the instantaneous polarization", Appl. Phys. Lett., V. 85, No. 13, p. 2463-2465 (2004).

2. **R. Adomavičius, A. Urbanowicz, G. Molis, A. Krotkus,** "Terahertz emission from narrow gap semiconductors photoexcited by femtosecond laser pulses", *Acta Physica Polonica,* V. 107, No. 1, p.132-136 (2005).

3. **R. Adomavičius, A. Urbanowicz, G. Molis and A. Krotkus , "**Terahertz radiation from narrow-gap semiconductors photoexcited by femtosecond laser pulses" *Microelectronic Engineering, , Available online 28 April 2005,*

4. **R. Adomavičius, G. Molis, A. Krotkus, and V. Sirutkaitis**, „Spectral dependencies of terahertz emission from InAs and InSb", Appl. Phys. Lett., (submitted).

5. **A. Krotkus, R. Adomavičius, and V. L. Malevich**, „Terahertz emission from semiconductor surfaces illuminated by femtosecond laser pulses", SPIE Proceedings, *ICONO – International Conference on Nonlinear Optics, St. Petersburg, Russia, May 11-15, 2005* (accepted for publication).

6. **R. Adomavičius, A. Urbanowicz, G. Molis, A. Krotkus;** "Terahertz radiation from narrow gap semiconductors photoexcited by femtosecond laser pulses",; *Symp. and Summer School "Nano and Giga Challenges in Microelectronics. Research and Development Opportunities", Cracow, Poland, Sept. 13-17, 2004, Abstracts*

7. **A. Urbanowicz, R. Adomavičius, and A. Krotkus**, „Terahertz emission from photoexcited surfaces of Ge crystals", Physica B (accepted for publication).

8. **A. Krotkus, R. Adomavičius, A. Urbanowicz, G. Molis, V. L. Malevich,**" Influences of photo-Dember effect and optical rectification on terahetz emission from narrow-gap semiconductor surfaces", *12th International Conference on Narrow-Gap Semiconductors, Toulouse, France, July 3-6, 2005 Abstracts*, p. 88.